

# Electrostatic Assembly Guided Synthesis of Highly Luminescent Carbon-Nanodots@BaSO<sub>4</sub> Hybrid Phosphors with Improved Stability

Ding Zhou, Yuechen Zhai, Songnan Qu,\* Di Li, Pengtao Jing, Wenyu Ji, Dezhen Shen, and Andrey L. Rogach

*Carbon nanodots (CNDs)@BaSO<sub>4</sub> hybrid phosphors are fabricated in an easy and low-cost process by sequentially assembling Ba<sup>2+</sup> and SO<sub>4</sub><sup>2-</sup> ions onto the surface of carbon nanodots through electrostatic attraction. CNDs act as the nucleus to attract these reactive ions and provide the luminescent centers in the hybrid phosphors. This strategy is versatile for a variety of negatively charged CNDs with different emission colors. The advantage of the resultant hybrid phosphors is that their luminescence exhibits excellent thermal and photostability, as well as remarkable resistance to strong acid/alkali and common organic solvents. These merits allow for the fabrication of CNDs-based light-emitting diodes using the CNDs@BaSO<sub>4</sub> hybrid phosphors as a color conversion layer.*

## 1. Introduction

With respect to traditional lighting, including tungsten halogen, metal halide, sodium, and compact fluorescent lamps, solid-state fluorescent materials-based white light emitting diodes (WLEDs) show significant promise in meeting the challenge of saving energy.<sup>[1]</sup> Solid-state fluorescent phosphors employed as a color conversion layer of WLEDs, play the key role in determining the performance of commercial light emitting diodes (LEDs), such as cost, emitting color,

luminous efficacy, color rendering index, color temperature, and so forth. However, conventional rare-earth-based phosphors are nonrenewable.<sup>[2]</sup> Semiconductor quantum dots (QDs) have been considered as potential alternative for LEDs,<sup>[3]</sup> but the high-performance QDs are often Cd based, leading to toxicity concerns.<sup>[4]</sup> Consequently, finding alternative materials, which could be easily prepared in a large scale by the widely available precursors, for substituting rare-earth-based phosphors or Cd<sup>2+</sup>-based QDs is an important research avenue in developing LEDs.

Carbon nanodots (CNDs), an emerging class of carbon-based luminescent nanomaterials, have drawn increasing attention owing to their extensive applications in various fields, such as bioimaging, biosensors, optoelectronics, laser, catalysis, and so forth.<sup>[5–27]</sup> CNDs possess several distinct merits, such as tunable emission, high photostability, low cost, and low cytotoxicity.<sup>[28–35]</sup> Thus, CNDs-based phosphors are desirable as a color conversion layer in LEDs.<sup>[36–44]</sup> However, efficient CNDs-based solid-state luminescent materials, as a class of potential phosphors, are difficult to realize. This is mainly because of the aggregation-induced luminescence quenching of CNDs in the solid state, which deteriorate their photoluminescence (PL) properties.<sup>[45,46]</sup> To overcome this issue, several encapsulation methods of CNDs based on the physical adsorption have been proposed.<sup>[36–41]</sup> In our previous work, environmental friendly phosphors based on CNDs and

Dr. D. Zhou, Dr. Y. C. Zhai, Prof. S. N. Qu,  
Dr. D. Li, Dr. P. T. Jing, Dr. W. Y. Ji, Prof. D. Z. Shen  
State Key Laboratory of Luminescence and  
Applications

Changchun Institute of Optics  
Fine Mechanics and Physics  
Chinese Academy of Sciences  
Changchun 130033, China  
E-mail: qusn@ciomp.ac.cn

Prof. A. L. Rogach  
Department of Physics and Materials Science  
and Centre for Functional Photonics (CFP)  
City University of Hong Kong  
Kowloon, Hong Kong SAR

DOI: 10.1002/sml.201602055



starch composites were synthesized.<sup>[39]</sup> Although the intense PL emission of the CNDs was well preserved in the solid state, the thermal stability of these phosphors was proved to be poor due to the thermally instable organic starch matrix. Besides the organic matrix, inorganic salt (NaCl) was also utilized to stabilize the PL properties of CNDs.<sup>[40]</sup> NaCl could protect CNDs from the destruction under UV irradiation and heat for a long time through isolating them from atmospheric oxygen. However, NaCl-embedded CNDs do not possess resistance to water, acids or alkali, which restrict the application fields of the NaCl-embedded CNDs, such as lighting in water. Similarly, CNDs were encapsulated by polyhedral oligomeric silsesquioxane.<sup>[38]</sup> The resulting composites had a high photoluminescence quantum yield (PLQY) of up to 60%, but they were still not resistive to water. Thus, it is still an urgent need to develop a new concept of preparing highly luminescent CNDs-based phosphors with improved thermal and photostability and resistance to different solvents.

In order to achieve the aim, we propose a fabrication method toward strongly luminescent and stable CNDs-based hybrid phosphors through electrostatic assembly conducted process. First, CNDs with negative charges on the surface are selected. After adding  $\text{BaCl}_2$ ,  $\text{Ba}^{2+}$  ions can be attracted onto the surface of CNDs through electrostatic interaction. Likewise, through the addition of  $\text{Na}_2\text{SO}_4$ ,  $\text{SO}_4^{2-}$  ions can be attracted by the  $\text{Ba}^{2+}$  ions absorbed on the surface of CNDs, leading to the growth of  $\text{BaSO}_4$  around the CNDs nucleus, which further fuse to form nanosized CNDs@ $\text{BaSO}_4$  hybrid phosphors (Figure 1). Being different from the previously reported encapsulation strategies relying on physical adsorption, the resultant CNDs@ $\text{BaSO}_4$  hybrid phosphors are formed through electrostatic interaction leading to the chemical reaction.  $\text{BaSO}_4$  matrix provides an environmentally friendly, low-cost, and stable material, useful to realize hybrid phosphors with high stability and strong luminescence. By virtue of the inorganic nature of  $\text{BaSO}_4$ , the resultant hybrid phosphors possess excellent thermal stability (up to 300 °C) and photostability, as well as high resistance to different solvents (strong acid/alkali and common organic solvents), ensuring the PL stability upon mixing with various packaging materials. These advantages permit the fabrication of

CNDs-based LEDs with tunable Commission Internationale de L'Eclairage (CIE) coordinates using the hybrid phosphors as a color conversion layer on a blue emitting InGaN chip.

## 2. Results and Discussion

CNDs with green emission are synthesized via a microwave-assisted strategy according to our previous work.<sup>[16]</sup> To obtain more uniform-sized CNDs, the as-prepared CNDs solutions are further dialyzed in deionized water using a membrane for 2 d. The purified CNDs with green emission (hereafter, referred as g-CND) show an absorbance peak located at 410 nm, which is narrower than that of initial CNDs, indicating their narrowed size distribution (Figure S1a, Supporting Information), which is also demonstrated by transmission electron microscopy (TEM) and atomic force microscopy (Figure S1c,d, Supporting Information). The high-resolution TEM (HRTEM) image indicates that the interplanar distance of g-CND is 0.33 nm, consistent with the previously reported ones (Figure S1e, Supporting Information).<sup>[16]</sup> The PL emission spectrum and the excitation–emission matrix of g-CND in aqueous solution exhibit a peak centered at 522 nm when excited by 405 nm light (Figure S1a,b, Supporting Information). The PLQYs of dialyzed g-CND is 17%, slightly higher than that of initial CNDs (15%).

Since there are plenty of carboxyl and hydroxyl groups in g-CND, which has been proved through Fourier transform infrared spectroscopy in our previous report,<sup>[39]</sup> g-CND possess negative charge on the surface (Figure 1). The zeta potential of g-CND in aqueous solution is measured to be  $-32$  mV. To achieve highly luminescent phosphors, g-CND aqueous solution is first premixed with  $\text{BaCl}_2$ .  $\text{Ba}^{2+}$  ions are attracted on the surface of g-CND through electrostatic interaction (Figure 1). The zeta potential of the  $\text{Ba}^{2+}$ -treated g-CND changes to  $+6$  mV, indicating that  $\text{Ba}^{2+}$  ions are indeed attached onto the surface of g-CND, which would favor further electrostatic assembly between  $\text{Ba}^{2+}$ -surrounded g-CND and  $\text{SO}_4^{2-}$  ions. After adding  $\text{Na}_2\text{SO}_4$  aqueous solution,  $\text{SO}_4^{2-}$  ions are attracted by  $\text{Ba}^{2+}$  ions on the surface of g-CND, leading to the in situ formation of  $\text{BaSO}_4$ -host nanoparticles

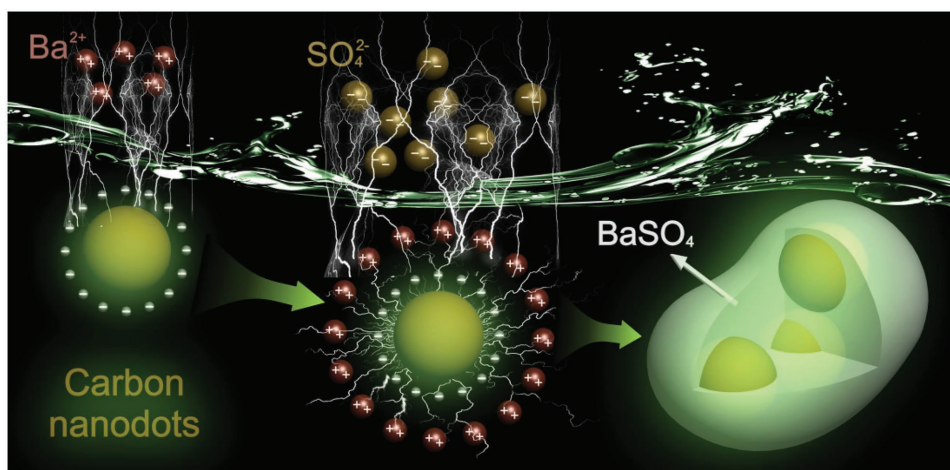
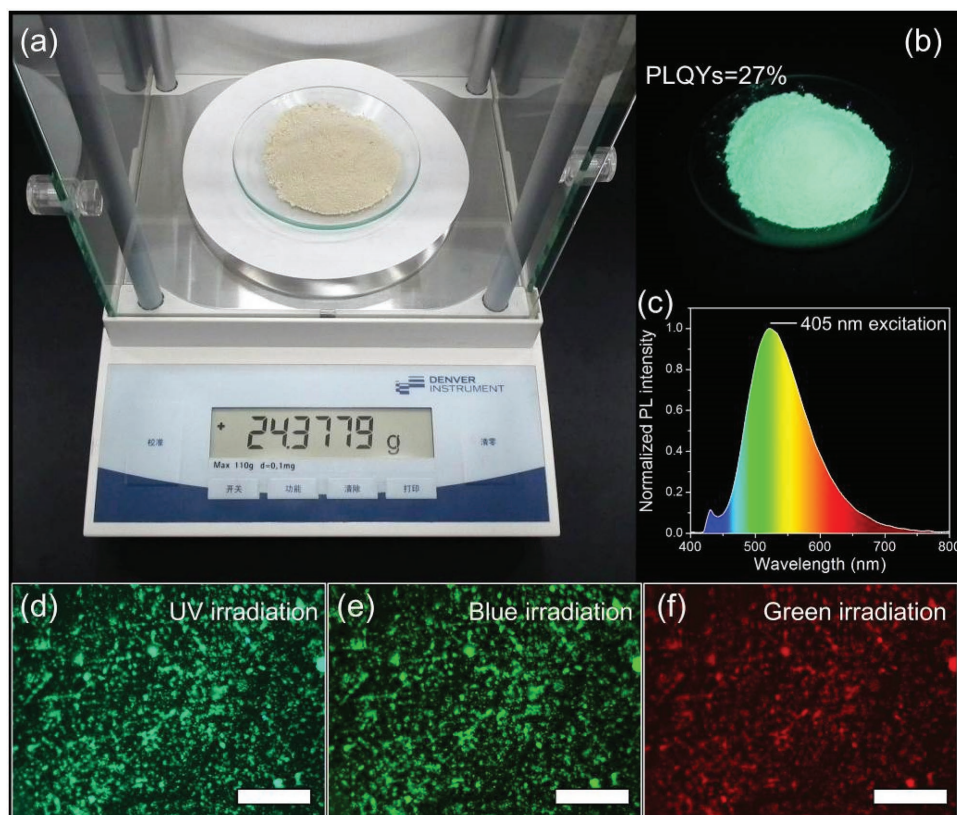


Figure 1. Schematics of the fabrication of CNDs@ $\text{BaSO}_4$  hybrid phosphors.



**Figure 2.** a) Optical and b) fluorescence images of g-CND@BaSO<sub>4</sub> hybrid phosphors taken under sunlight and UV light, respectively. c) The corresponding PL spectrum taken at 405 nm excitation. Fluorescence images are observed through fluorescence microscope under d) UV, e) blue, and f) green excitation, respectively. The exposure time is b) 100, c) 200, and d) 6000 ms. The scale bar is 50  $\mu$ m.

embedding g-CND (Figure 1). During this process, g-CND, as the nucleus, stepwise attracts reactive ions, and it finally leads to the formation of g-CND@BaSO<sub>4</sub> phosphors. By this simple approach, we could easily prepare more than 20 g of g-CND@BaSO<sub>4</sub> hybrid phosphors in one pot, where the reaction time to form g-CND@BaSO<sub>4</sub> hybrid phosphors is less than 5 min (Figure 2a). Under UV light, the hybrid phosphors exhibit bright turquoise fluorescence from the embedded g-CND (Figure 2b,d), whereas bare BaSO<sub>4</sub> precipitate obtained by mixing BaCl<sub>2</sub> and Na<sub>2</sub>SO<sub>4</sub> has no PL emission (Figure S2, Supporting Information). Under 405 nm excitation, the PL peak of the g-CND@BaSO<sub>4</sub> hybrid phosphors is located at 520 nm with PLQYs of 27% (Figure 2b,c). The enhanced PLQYs of the hybrid phosphors is mainly due to less energy loss compared with g-CND aqueous solution, which can be further demonstrated by comparing their PL decay curves (Figure S3, Supporting Information).<sup>[39]</sup> As shown in Figure S3 (Supporting Information), the luminescence lifetime of the hybrid phosphors is longer than that of g-CND aqueous solution. These facts indicate that g-CND can be well separately embedded and protected by the BaSO<sub>4</sub> host during the electrostatic assembly conducted process, which can effectively avoid energy loss induced by water molecules, leading to increased PLQYs.<sup>[39]</sup> These results point out on the preservation and even improvement of PL properties of g-CND in the inorganic hybrid phosphors. Likewise, as one of the attracting properties of CNDs, the excitation-dependent PL emission behavior is also preserved in the

g-CND@BaSO<sub>4</sub> hybrid phosphors. The fluorescent colors are turquoise, green, and red, when changing the excitation light from UV to blue, and green light (Figure 2d–f).

To further characterize the structure of hybrid phosphors, TEM and scanning electron microscope (SEM) studies are carried out. TEM and SEM reveal that the g-CND@BaSO<sub>4</sub> hybrid phosphors have a size of 60–150 nm (Figure 3a–c). In the HRTEM image (Figure 3b), large areas of interplanar distance are 0.21 nm, which should belong to BaSO<sub>4</sub>. Carefully observing, there are small areas with interplanar distance of 0.33 nm, which should belong to g-CND (Figure S1e, Supporting Information), and is marked in a circle dot line.<sup>[16]</sup> Bare BaSO<sub>4</sub> precipitate prepared by mixing BaCl<sub>2</sub> and Na<sub>2</sub>SO<sub>4</sub> aqueous solutions has much larger diameters and broader size distribution (Figure S2c, Supporting Information). The difference in size is attributed to the presence of g-CND, which act as nucleus in the electrostatic assembly process, leading to a more uniform size distribution and smaller size of BaSO<sub>4</sub> particles. X-ray powder diffraction (XRD) patterns indicate that the lattice parameters of the g-CND@BaSO<sub>4</sub> hybrid phosphors fit well to the orthorhombic structure of bulk crystalline BaSO<sub>4</sub> powder (Figure S4, Supporting Information). There are no characteristic diffraction peaks of g-CND in the XRD pattern, as they are rather weak and overlap with those of crystalline BaSO<sub>4</sub> (Figure S4, Supporting Information). Energy-dispersive spectrum (EDS) and mapping images confirm the existence of C and N elements (Figure 3d; Figure S5, Supporting

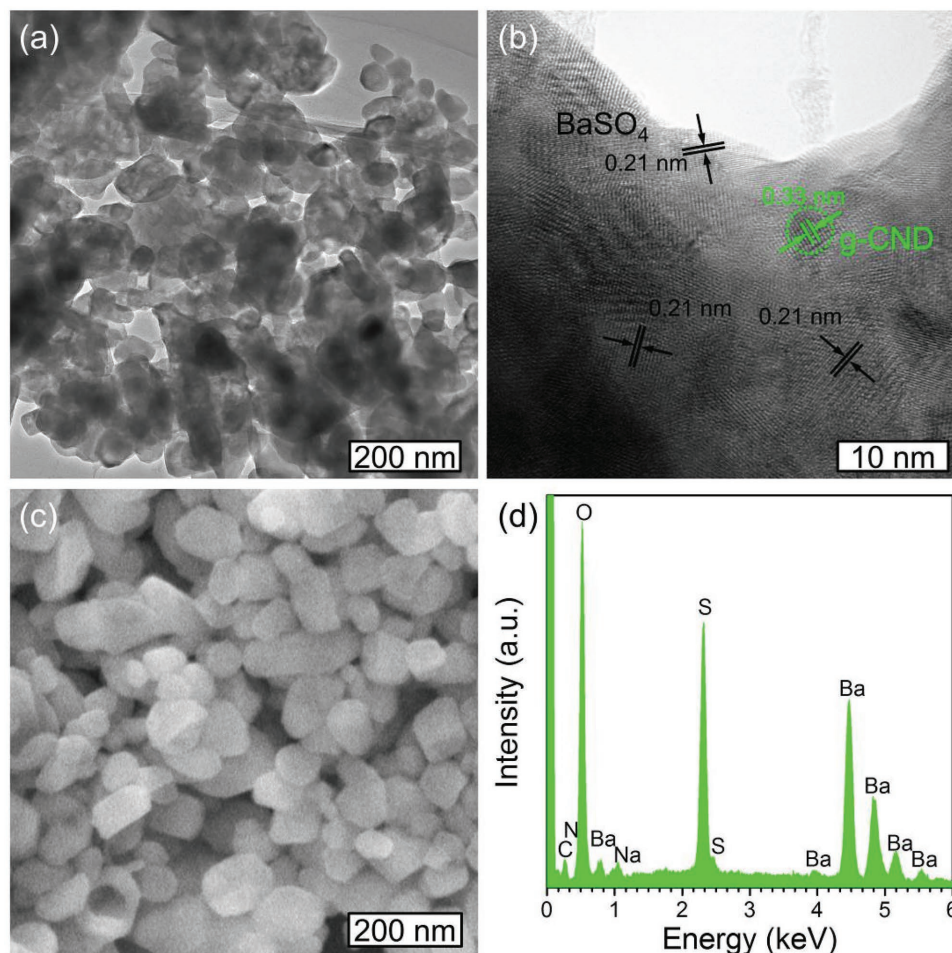


**Figure 3.** a) TEM image, b) HRTEM image, c) SEM image, and d) EDS pattern of g-CND@BaSO<sub>4</sub> hybrid phosphors.

Information), which is originating from g-CND synthesized from citric acid and urea.<sup>[16]</sup> According to the EDS analysis, the fraction of carbon atoms in the hybrid phosphors is about 8% and (atomic ratio), and the weight ratio of g-CND in the hybrid phosphors is calculated to be higher than 5.6% (Figure S6, Supporting Information). Furthermore, X-ray photoelectron spectroscopy (XPS) characterizations also demonstrate the existence of g-CND in the hybrid phosphors (Figure S7, Supporting Information).

To further prove the importance of the electrostatic assembly conducted process, the sequence of adding BaCl<sub>2</sub> and Na<sub>2</sub>SO<sub>4</sub> is changed, where Na<sub>2</sub>SO<sub>4</sub> is first added. Under this condition, the resultant product has low g-CND loading fraction and broad size distribution (Figure S8, Supporting Information). Under a same excitation light source, the PL emission of this resultant product is weaker than that of g-CND@BaSO<sub>4</sub> hybrid phosphors synthesized from electrostatic assembly conducted process (Figure S8a, Supporting Information). This is mainly because SO<sub>4</sub><sup>2-</sup> ions cannot be attracted by g-CND, leading to reduction in g-CND loading fraction (Table S1, Supporting Information). Meanwhile, owing to the different g-CND loading fractions, PL intensity differences become more and more obvious when increasing the intensity of the excitation light. We have measured their PL emission spectra under the same excitation light source

but varying the intensity of excitation light as shown in Figure S9 (Supporting Information). When the excitation light is weak, the PL intensity of the composites from first addition of BaCl<sub>2</sub> is about 1.2 times stronger than that of the composites from first addition of Na<sub>2</sub>SO<sub>4</sub> (Figure S9a, Supporting Information). As the intensity of excitation light increases, the absorbance of the composites from first addition of Na<sub>2</sub>SO<sub>4</sub> is almost saturated because of low g-CND loading fraction, so the PL intensity of the composites from first addition of BaCl<sub>2</sub> is about two times stronger than that of first addition of Na<sub>2</sub>SO<sub>4</sub> (Figure S9b, Supporting Information). When the intensity of excitation light further increases, the PL intensity of first addition of Na<sub>2</sub>SO<sub>4</sub> is nearly unchanged, whereas the PL intensity of first addition of BaCl<sub>2</sub> can be further enhanced, leading to nearly three times enhancement of PL intensity (Figure S9c, Supporting Information). These results demonstrate that there is a big difference in the g-CND loading fraction if changing the adding sequence of the BaCl<sub>2</sub> and Na<sub>2</sub>SO<sub>4</sub>, especially leading to significantly different PL intensities. Likewise, owing to the absence of g-CND nucleus, the size distribution of the product becomes broader than that of g-CND@BaSO<sub>4</sub> hybrid phosphors synthesized from electrostatic assembly conducted process (Figure 3c; Figure S8b, Supporting Information).

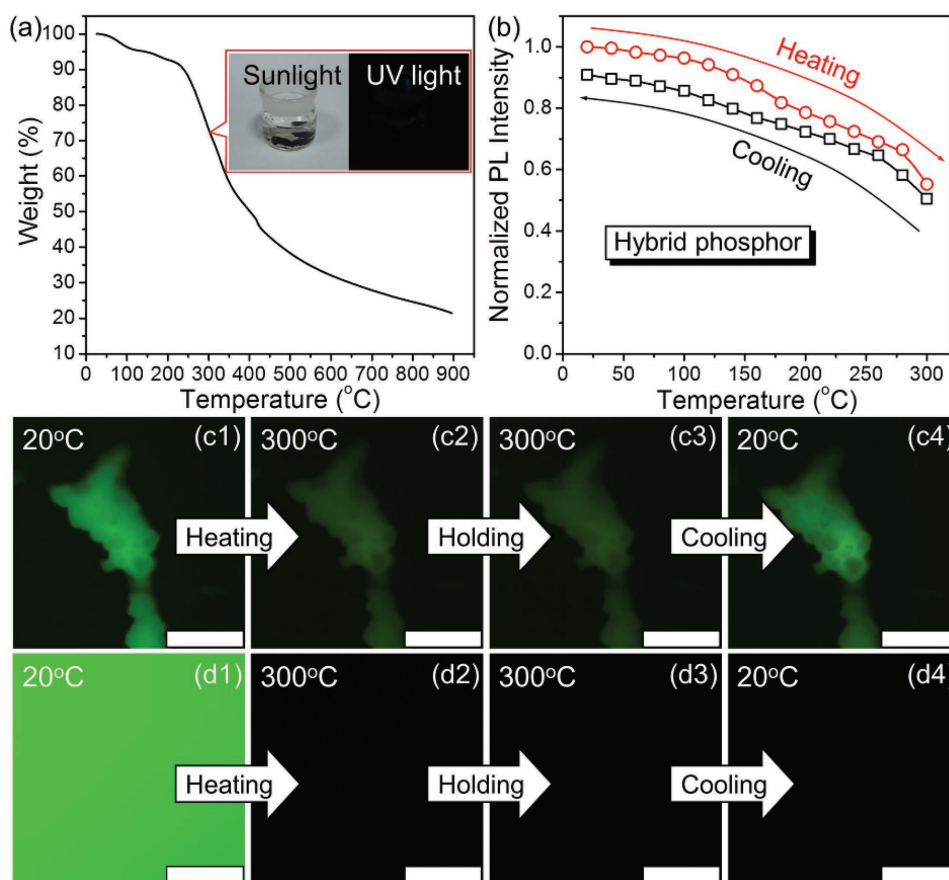


**Figure 4.** Comparison of the thermal stability among g-CND, g-CND@BaSO<sub>4</sub> hybrid phosphors, and commercial fluorescein sodium. a) TGA thermogram of the initial g-CND. Insets in (a) are photographs of pure g-CND powders after being heated at 300 °C for 30 min. b) Variation of the in situ measured PL intensity of the g-CND@BaSO<sub>4</sub> hybrid phosphors versus temperature. The temperature is increased from 20 to 300 °C in steps of 20 °C (red circles); after storing the sample at 300 °C for 30 min, it is cooled down to room temperature (black squares). Solid lines are solely provided as a guide to the eye. Fluorescence images of c) the g-CND@BaSO<sub>4</sub> hybrid phosphors, and d) fluorescein sodium versus temperature. The scale bar is 100 μm.

Thermogravimetric analysis (TGA) data reveal a weight loss in pure g-CND powders for the temperature exceeding 200 °C, indicating the dehydration and carbonization of the surface groups of g-CND (Figure 4a). After heating at 300 °C for 30 min, the resultant product becomes completely insoluble in water, and neither the product nor the solution shows any PL (insets in Figure 4a). On the contrary, g-CND@BaSO<sub>4</sub> hybrid phosphors exhibit excellent thermal stability (Figure S10, Supporting Information). When the temperature is 300 °C, only 0.1% weight loss occurs for the hybrid phosphors. According to further calculation, the weight loss of g-CND in the hybrid phosphors should be less than 1.7% (Figure S10, Supporting Information). To quantitatively analyze their thermally induced PL variations, the PL emission of the g-CND@BaSO<sub>4</sub> hybrid phosphors is examined in situ by the fluorescence microscope equipped with a spectrometer (Figure 4b,c). As shown in Figure 4b, when the temperature increases from 20 to 300 °C, the PL intensity of the g-CND@BaSO<sub>4</sub> hybrid phosphors is about 45% lower at 300 °C than at 20 °C. This loss is mainly due to high temperature-induced PL quenching.<sup>[47,48]</sup> After storing at 300 °C for 30 min, the g-CND@BaSO<sub>4</sub> hybrid phosphors are further cooled to room temperature, and their PL intensity recovers to over 90%

(Figure 4b). Their corresponding fluorescence images under blue light excitation at different temperatures are shown in Figure 4c. The apparent PL brightness variations of g-CND@BaSO<sub>4</sub> hybrid phosphors are well consistent with the data in Figure 4b. To compare thermal stability g-CND@BaSO<sub>4</sub> hybrid phosphors with other fluorescent materials, temperature-dependent PL property of the commercial fluorescein sodium is also investigated (Figure 4d). The fluorescence images of the fluorescein sodium show that their PL emission is almost completely quenched when raising the temperature up to 300 °C, and when the temperature is returned back to 20 °C, the PL emission is not restored (Figure 4d). To further prove the good thermal stability of g-CND@BaSO<sub>4</sub> hybrid phosphors, variation of the PL intensity of the hybrid phosphors during the temperature recycle between 20 °C (circle) and 300 °C (square) is shown below. In each recycle, the PL intensities are measured after storing the hybrid phosphors for 30 min. After several cycles, the PL intensity of the hybrid phosphors can still recover to 88% (Figure S11, Supporting Information). In addition, the low temperature resistance of the g-CND@BaSO<sub>4</sub> hybrid phosphors is tested in liquid nitrogen (Figure S12, Supporting Information). The PL colors are nearly identical before and after the treatment with liquid

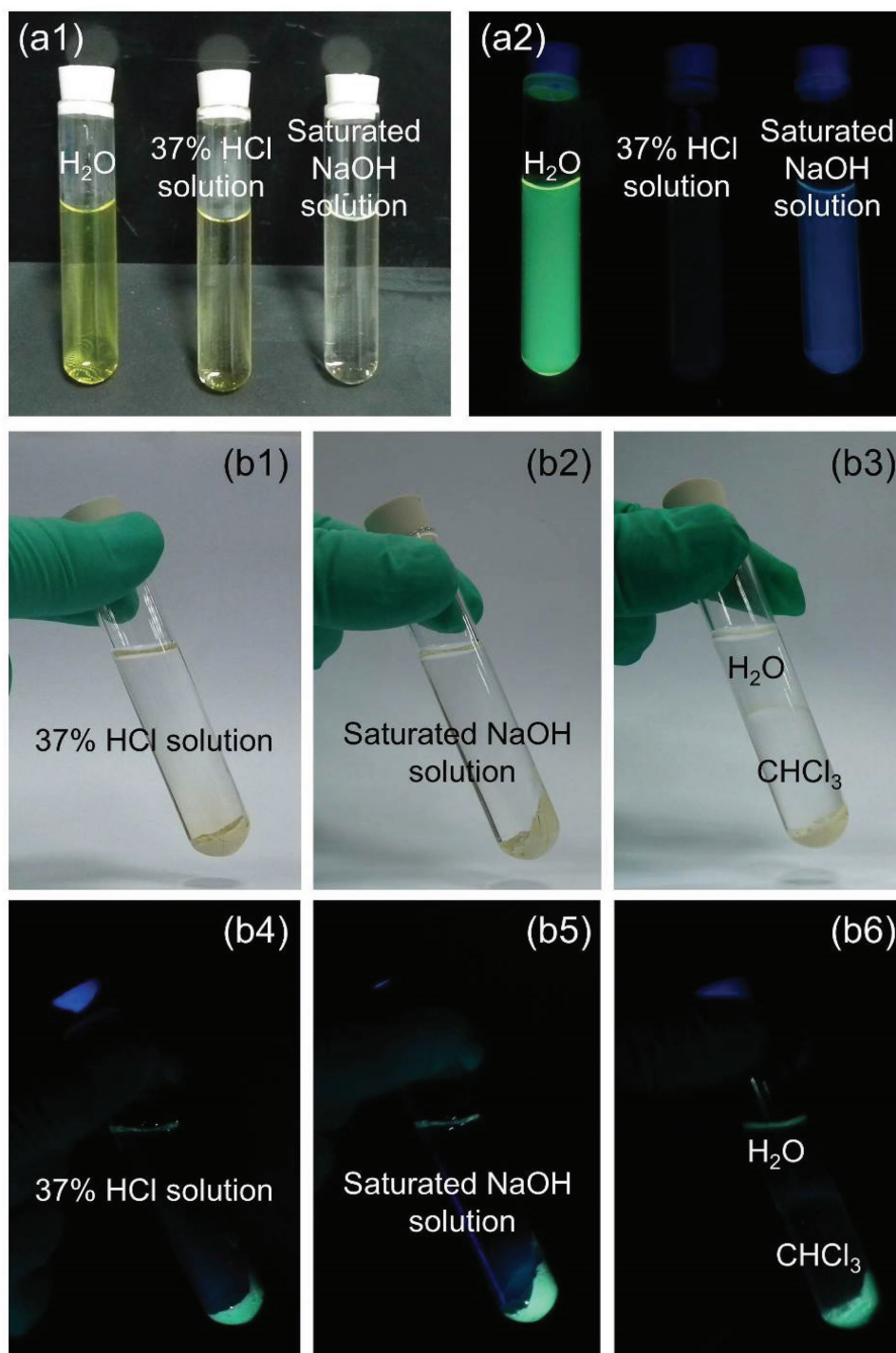


**Figure 5.** a) Stability of g-CND in water, concentrated HCl (37%), and saturated NaOH aqueous solutions. b) Stability of g-CND@BaSO<sub>4</sub> hybrid phosphors in concentrated HCl (37%), saturated NaOH aqueous solutions, and CHCl<sub>3</sub>. a1,b1–b3) Optical images. a2,b4–b6) Fluorescence images.

nitrogen (Figure S12b,d, Supporting Information), indicating high resistance to low temperature.

Under protection of BaSO<sub>4</sub> host, the hybrid phosphors possess resistance toward concentrated HCl (37%), saturated NaOH aqueous solutions, and organic solvents. First, equivalent bare g-CND is dispersed into deionized water, concentrated HCl, and saturated NaOH aqueous solutions, respectively (Figure 5a). g-CND dissolved in water possess a bright yellow color, whereas those dispersed in HCl aqueous

solution only exhibit shallow yellow color, and become colorless in NaOH aqueous solution (Figure 5a1). g-CND aqueous solution emits strong green fluorescence under UV light excitation, while those dispersed in HCl and NaOH aqueous solutions show very weak PL emission (Figure 5a2). In contrast, the PL emission of the g-CND@BaSO<sub>4</sub> hybrid phosphors does not change in concentrated HCl (37%) and saturated NaOH aqueous solutions (Figure 5b), indicating the much better stability of the hybrid phosphors. In addition,

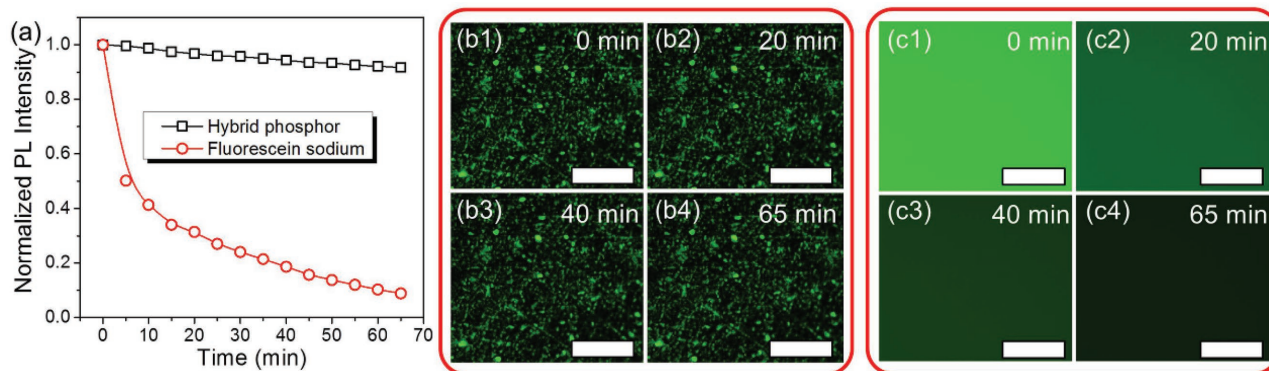


**Figure 6.** a) Evolution of the PL intensity of g-CND@BaSO<sub>4</sub> hybrid phosphors (black squares), and commercial fluorescein sodium (red circles), under UV light (1.6 W cm<sup>-2</sup>). Solid lines are solely provided as a guide to the eye. Variation of the fluorescence images of b) g-CND@BaSO<sub>4</sub> hybrid phosphors, and c) commercial fluorescein sodium versus irradiation duration. The scale bar is 50 μm.

they cannot be dissolved or swollen by common organic solvents, such as chloroform, toluene, benzene, acetone, ethanol, and dimethylformamide (Figure 5b3,b6; Figure S13, Supporting Information). After being soaked in above solvents for 3 d, the PL emission spectra of each supernatant solution are measured after centrifugation at a speed of 6000 rpm for 5 min. No PL emissions are observed, indicating insolubility of the hybrid phosphors in these solvents (Figure 5; Figure S13, Supporting Information). It is worth mentioning that since the dissolved g-CND in water cannot be separated at all by centrifugation at a speed of 6000 rpm for 5 min (Figure S14, Supporting Information), the centrifugal process can only remove the suspended hybrid phosphors but not the dissolved g-CND. The excellent solvent resistance of the g-CND@BaSO<sub>4</sub> hybrid phosphors ensures their PL stability upon mixing with various packaging materials when processed toward LEDs.

The g-CND@BaSO<sub>4</sub> hybrid phosphors are also resistant against UV light irradiation. The photostability is investigated by comparing the PL intensity of the samples, including g-CND@BaSO<sub>4</sub> hybrid phosphors and commercial fluorescein sodium, which are continuously irradiated by a UV light (1.6 W cm<sup>-2</sup>) under the same conditions. As seen from **Figure 6a**, the harsh conditions of the irradiation used in our tests are indeed harmful to all of the samples. Fluorescein sodium losses more than a half of its initial PL intensity after the first 5 min of irradiation, and its PL is almost completely quenched after 65 min of irradiation. On the contrary, the PL intensity of g-CND@BaSO<sub>4</sub> hybrid phosphors is preserved by more than 90% even after 65 min of irradiation (Figure 6a).

Our encapsulation method is universal to any CNDs with negative surface charges and different PL emission colors. For instance, CNDs with blue PL emission (b-CND) are prepared according to our previous report (Figure S15, Supporting Information).<sup>[49]</sup> The zeta potential of b-CND in aqueous solution is measured to be about -30 mV. Then, aqueous b-CND solutions are mixed with BaCl<sub>2</sub>, after which Na<sub>2</sub>SO<sub>4</sub> is added into the mixture, leading to the formation of b-CND@BaSO<sub>4</sub> hybrid phosphors (Figure S16, Supporting Information). Under fluorescence microscope, the hybrid phosphors exhibit blue, green, and red emissions, respectively,

when changing the excitation light from UV to blue, and green (Figure S16b–d, Supporting Information).

Based on the advantageous properties of CNDs@BaSO<sub>4</sub> hybrid phosphors demonstrated above, including excellent thermal stability, high resistance toward different solvents and UV light, and the excitation tunable PL emission, we applied them as phosphors in down-conversion LEDs. Mixtures of g-CND@BaSO<sub>4</sub> hybrid phosphors and polydimethylsiloxane (PDMS) precursor solution with different ratios ranging from 3:1 to 0.1:1 wt% are deposited on commercially available 0.2 W InGaN LED chips, and cured in an oven at 80 °C for 1 h. Through adjusting the contents of the hybrid phosphors in the mixtures, PL reabsorption among g-CND could be controlled, and therewith LEDs with different CIE coordinates are obtained (**Figure 7**). To confirm this proposal, two blocks of mixtures of the hybrid phosphors and PDMS with different mass ratios (0.1:1 and 3:1 wt%) but same thickness are prepared. As shown in Figure S17b (Supporting Information), the PL emission colors of these two blocks are nearly identical from the same side view with a UV lamp, indicating that these two blocks preserve the PL properties of the hybrid phosphors without further aggregating of g-CND. Then, the two blocks are placed between excitation light source and detector to compare their PL properties (Figure S17c–g, Supporting Information). Due to the overlap between the PL emission and absorbance of g-CND (Figure S1a, Supporting Information), the high energy emission (i.e., shorter wavelength) from the hybrid phosphors near to the excitation light source could be progressively absorbed along the path of light transmission. The higher the mass ratio of the hybrid phosphors leads to more obvious reabsorption (Figure S17e,f, Supporting Information). As a result, the PL emission spectrum of the block with high mass ratio of the hybrid phosphors possesses an obvious red-shift compared with that of low mass ratio of the hybrid phosphors (Figure S17g, Supporting Information). These results clearly indicate that the emission reabsorption becomes stronger as increasing mass ratio of the hybrid phosphors. In LEDs, the InGaN chip and emission detector are placed on different sides of the mixture of the hybrid phosphors and PDMS. Similarly, PL reabsorption can be also observed through the emission spectra of LEDs (insets in Figure 7a–e),

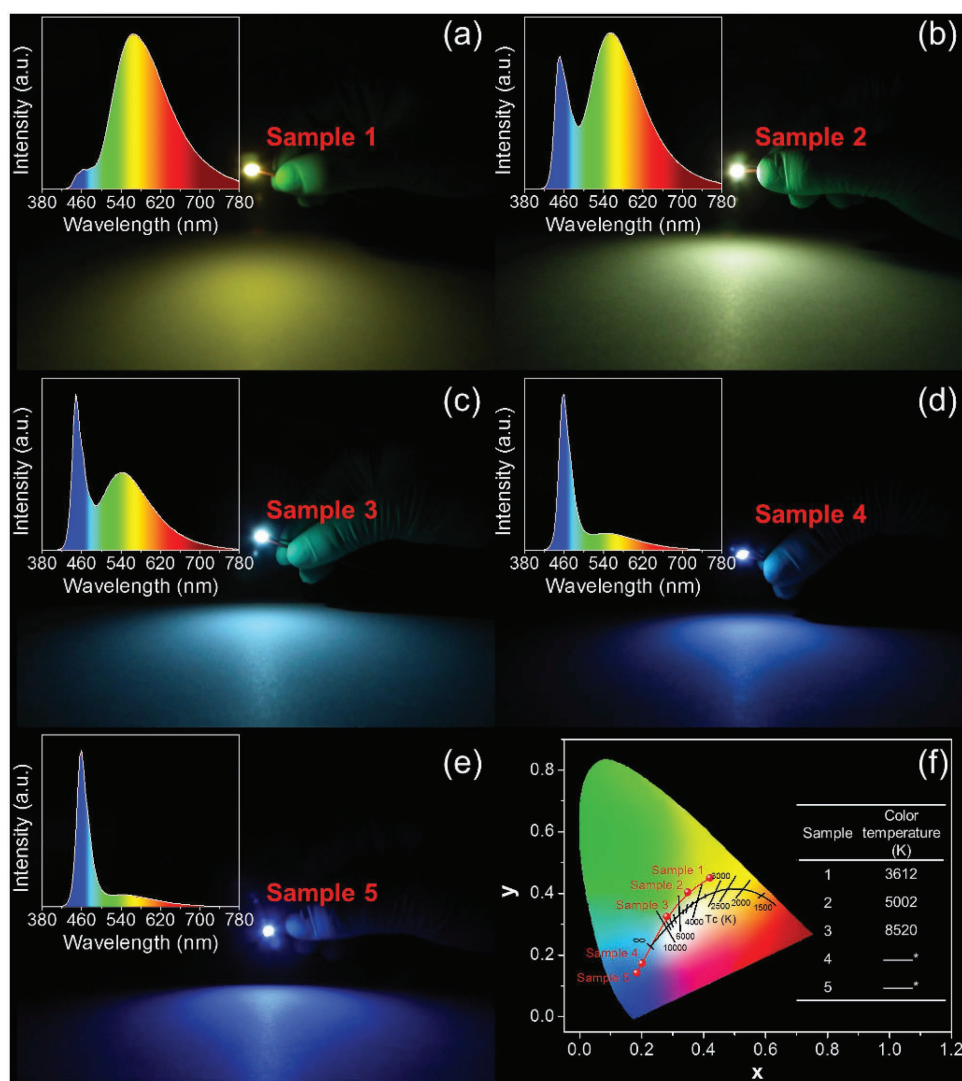


**Figure 7.** Photographs of the working LED prototypes with different color temperatures, where the mass ratios of g-CND@BaSO<sub>4</sub> hybrid phosphors to PDMS are a) 3:1, b) 2:1, c) 1:1, d) 0.5:1, and e) 0.1:1, respectively. Insets in (a–e) are the corresponding emission spectra of LEDs. f) CIE chromaticity diagram showing (x,y) color coordinates of the five LEDs. The black curve represents the variation of color temperature with the color coordinates. The points on the black straight line are constant color temperature. The color temperatures of samples 4 and 5 are too high to be calculated.

where the emission peaks red-shift upon increasing the contents of hybrid phosphors.<sup>[50]</sup> The high energy emissions from the g-CND@BaSO<sub>4</sub> hybrid phosphors near to the InGaN chip could be progressively absorbed by the outer g-CND@BaSO<sub>4</sub> hybrid phosphors along the output emission path. Therefore, increasing the hybrid phosphors concentrations results in higher probability of the reabsorption among g-CND@BaSO<sub>4</sub> hybrid phosphors through the color conversion layer, leading to the obvious red-shifted emission spectra (insets in Figure 7a–e).<sup>[51,52]</sup> As seen from Figure 7b, a white LED prototype based entirely on g-CND@BaSO<sub>4</sub> is achieved, with CIE coordinates, color temperature, color rendering index, luminous efficacy of optical radiation, and luminous efficiency is (0.34, 0.39), 5002 K, 72, 21 lm W<sup>-1</sup> and 11%, respectively. When increasing the hybrid phosphors concentrations, a warm white LED prototype is achieved, whose CIE coordinates and color temperature is (0.42, 0.45) and 3612 K (Figure 7a), respectively. Correspondingly,

several other LEDs with different color temperatures could be obtained by reducing the amount of the hybrid phosphors in the deposited layer (Figure 7c–e).

### 3. Conclusions

In summary, we fabricated CNDs@BaSO<sub>4</sub> hybrid phosphors via electrostatic assembly guided synthesis, where Ba<sup>2+</sup> ions are foremost attracted onto the negatively charged surface of CNDs, and react with SO<sub>4</sub><sup>2-</sup> ions to form BaSO<sub>4</sub> protective matrix. CNDs@BaSO<sub>4</sub> hybrid phosphors exhibit excellent thermal and photostability in terms of their PL emission, as well as remarkable resistance to strong acid/alkali and common organic solvents. The PL intensity of the hybrid phosphors could preserve 90% and 92% after storing at 300 °C for 30 min and continuous UV irradiations (1.6 W cm<sup>-2</sup>) for 1 h, respectively. This allows us to

fabricate LEDs with different CIE coordinates based on CNDs@BaSO<sub>4</sub> hybrid phosphors. Our synthetic methodology holds a promise for developing other hybrid phosphors well protected from the environment.

#### 4. Experimental Section

**Materials:** Citric acid (99.5%), BaCl<sub>2</sub>·2H<sub>2</sub>O (99.5%), Na<sub>2</sub>SO<sub>4</sub> (99%), NH<sub>3</sub>·H<sub>2</sub>O (≈25%), and urea (99%) were purchased from Aladdin. PDMS elastomer kits (Sylgard 184) were purchased from Dow Corning (Midland, MI). All chemicals were used without further purification.

**Synthesis and Purification of CNDs with Green Emission:** 3 g of citric acid and 6 g of urea were dissolved into 20 mL of deionized water. The mixture was heated in a domestic 750 W microwave oven for about 5 min, during which the color of the solution changed from a colorless liquid to a light brown and finally dark brown solid, indicating the formation of CNDs. The solid was redissolved in water and centrifuged to remove aggregated particles at a speed of 8000 rpm for 20 min three times. To further purify CNDs, the solution was dialyzed in deionized water using a membrane (MWCO = 0.1–0.5 KD, Spectrum Laboratories). Finally, the clear, yellow-brown g-CND solutions were obtained and freeze-dried for further use.

**Synthesis of CNDs with Blue Emission:** 3 g of citric acid was added into 20 mL of NH<sub>3</sub>·H<sub>2</sub>O. The mixture was heated in a domestic 750 W microwave oven for about 5 min, during which the color of the solution changed from a colorless liquid to brown and finally dark brown liquid, indicating the formation of CNDs. The products were diluted in aqueous solution and centrifuged to remove aggregated particles at a speed of 8000 rpm for 20 min three times.

**Preparation of CNDs@BaSO<sub>4</sub> Hybrid Phosphors:** 2.44 g of BaCl<sub>2</sub> was added into 10 mL of 2.5 mg mL<sup>-1</sup> CNDs aqueous solution, and the mixture was stirred for 3 min for a complete adsorption of Ba<sup>2+</sup> ions onto the surface of CNDs. 10 mL of 1 mol L<sup>-1</sup> Na<sub>2</sub>SO<sub>4</sub> aqueous solution was added under stirring, resulting in the formation of yellowish CNDs@BaSO<sub>4</sub> hybrid phosphors precipitate. For purification, the as-prepared CNDs@BaSO<sub>4</sub> hybrid phosphors were washed by water through centrifugation at 6000 rpm for 5 min three times.

**Fabrication of LEDs from the g-CND@BaSO<sub>4</sub> Hybrid Phosphors:** InGaN LED chips were purchased from Shen Zhen Hongcai Electronics CO., Ltd. The microchip, which emitted 450 nm light at the operating voltage of 3.0 V, was placed at the bottom of the LED base. For the preparation of the color conversion layer, the g-CND@BaSO<sub>4</sub> hybrid phosphors were foremost mixed with the PDMS precursors with different mass ratios of 3:1, 2:1, 1:1, 0.5:1, and 0.1:1, respectively. The mixtures were filled into the cup-shaped void of LED chip. After curing at 80 °C for 1 h, the LEDs based on the g-CND@BaSO<sub>4</sub> hybrid phosphors were obtained.

**Characterization:** UV–visible absorption spectra were obtained on a Shimadzu UV-3101PC spectrophotometer. PL spectra were collected on a Hitachi F-7000 spectrophotometer. The PLQYs of CNDs, g-CND aqueous solution, and g-CND@BaSO<sub>4</sub> hybrid phosphors were measured in a calibrated integrating sphere in FLS920 spectrometer under 405 nm excitation. TEM was performed on a FEI Tecnai-G2-F20 TEM at 200 kV. AFM measurements were

performed on a SA400HV with a Seiko SPI3800N controller. SEM was done on a JEOL FESEM 6700F electron microscope with primary electron energy of 3 kV. Time-resolved PL spectra were measured by a LifeSpec-II dedicated lifetime spectrometer (Edinburgh Instruments). EDS and elemental mapping were conducted on an Inca X-Max instrument (Oxford Instruments). XPS was investigated using a VG ESCALAB MKII spectrometer with a Mg KR excitation (1253.6 eV). Binding energy calibration was based on C 1s at 284.6 eV. Zeta potential measurements were performed on a Zetasizer Nano-ZS (Malvern Instruments). TGA was done on an American TA Q500 analyzer under N<sub>2</sub> atmosphere with the flow rate of 100 mL min<sup>-1</sup>. XRD measurements were carried out on a Siemens D5005 diffractometer. The fluorescence microscopy images were obtained on a C2+ confocal microscope system (Nikon confocal instruments).

#### Supporting Information

Supporting Information is available from the Wiley Online Library or from the author.

#### Acknowledgements

This work was supported by the National Natural Science Foundation of China (Grant Nos. 51602304, 61274126, 61306081, 51572128), Outstanding young scientists program of Chinese Academy of Sciences, Jilin Province Science and Technology Research Project Nos. 20160520008JH, 20140101060JC, 20150519003JH, 20130522142JH, and NPRP grant no. 8-878-1-172 from the Qatar National Research Fund (a member of the Qatar Foundation).

- [1] S. Landau, J. Erion, *Nat. Photonics* **2007**, *1*, 31.
- [2] Q. Q. Dai, C. E. Duty, M. Z. Hu, *Small* **2010**, *6*, 1577.
- [3] A. L. Rogach, N. Gaponik, J. M. Lupton, C. Bertoni, D. E. Gallardo, S. Dunn, N. L. Pira, M. Paderi, P. Repetto, S. G. Romanov, C. O'Dwyer, C. M. S. Torres, A. Eychmüller, *Angew. Chem., Int. Ed.* **2008**, *47*, 6538.
- [4] E. Jang, S. Jun, H. Jang, J. Lim, B. Kim, Y. Kim, *Adv. Mater.* **2010**, *22*, 3076.
- [5] H. Choi, S.-J. Ko, Y. Choi, P. Joo, T. Kim, B. R. Lee, J.-W. Jung, H. J. Choi, M. Cha, J.-R. Jeong, I.-W. Hwang, M. H. Song, B.-S. Kim, J. Y. Kim, *Nat. Photonics* **2013**, *7*, 732.
- [6] T. F. Yeh, C. Y. Teng, S. J. Chen, H. Teng, *Adv. Mater.* **2014**, *26*, 3297.
- [7] S. L. Hu, A. Trinchì, P. Atkin, I. Cole, *Angew. Chem., Int. Ed.* **2015**, *54*, 2970.
- [8] L. Bao, C. Liu, Z. L. Zhang, D. W. Pang, *Adv. Mater.* **2015**, *27*, 1663.
- [9] Y. P. Sun, B. Zhou, Y. Lin, W. Wang, K. A. S. Fernando, P. Pathak, M. J. Mezziani, B. A. Harruff, X. Wang, H. F. Wang, P. G. Luo, H. Yang, M. E. Kose, B. L. Chen, L. M. Veca, S. Y. Xie, *J. Am. Chem. Soc.* **2006**, *128*, 7756.
- [10] S. T. Yang, L. Cao, P. G. Luo, F. S. Lu, X. Wang, H. F. Wang, M. J. Mezziani, Y. F. Liu, G. Qi, Y. P. Sun, *J. Am. Chem. Soc.* **2009**, *131*, 11308.

- [11] L. Cao, X. Wang, M. J. Meziani, F. S. Lu, H. F. Wang, P. G. Luo, Y. Lin, B. A. Harruff, L. M. Veca, D. Murray, S. Y. Xie, Y. P. Sun, *J. Am. Chem. Soc.* **2007**, *129*, 11318.
- [12] B. Kong, A. W. Zhu, C. Q. Ding, X. M. Zhao, B. Li, Y. Tian, *Adv. Mater.* **2012**, *24*, 5844.
- [13] C. Q. Ding, A. W. Zhu, Y. Tian, *Acc. Chem. Res.* **2014**, *47*, 20.
- [14] S. J. Zhu, Q. N. Meng, L. Wang, J. H. Zhang, Y. B. Song, H. Jin, K. Zhang, H. C. Sun, H. Y. Wang, B. Yang, *Angew. Chem., Int. Ed.* **2013**, *52*, 3953.
- [15] X. Y. Zhang, Y. Zhang, Y. Wang, S. Kalytchuk, S. V. Kershaw, Y. H. Wang, P. Wang, T. Q. Zhang, Y. Zhao, H. Z. Zhang, T. Cui, Y. D. Wang, J. Zhao, W. W. Yu, A. L. Rogach, *ACS Nano* **2013**, *7*, 11234.
- [16] S. N. Qu, X. Y. Liu, X. Y. Guo, M. H. Chu, L. G. Zhang, D. Z. Shen, *Adv. Funct. Mater.* **2014**, *24*, 2689.
- [17] S. N. Baker, G. A. Baker, *Angew. Chem., Int. Ed.* **2010**, *49*, 6726.
- [18] S. Y. Lim, W. Shen, Z. Q. Gao, *Chem. Soc. Rev.* **2015**, *44*, 362.
- [19] W. Kwon, G. Lee, S. Do, T. Joo, S. W. Rhee, *Small* **2014**, *10*, 506.
- [20] X. Y. Xu, R. Ray, Y. L. Gu, H. J. Ploehn, L. Gearheart, K. Raker, W. A. Scrivens, *J. Am. Chem. Soc.* **2004**, *126*, 12736.
- [21] K. Jiang, S. Sun, L. Zhang, Y. Lu, A. G. Wu, C. Z. Cai, H. W. Lin, *Angew. Chem., Int. Ed.* **2015**, *54*, 5360.
- [22] J. G. Zhou, C. Booker, R. Y. Li, X. T. Zhou, T. K. Sham, X. L. Sun, Z. F. Ding, *J. Am. Chem. Soc.* **2007**, *129*, 744.
- [23] H. Ding, S. B. Yu, J. S. Wei, H. M. Xiong, *ACS Nano* **2016**, *10*, 484.
- [24] F. Wang, Y. H. Chen, C. Y. Liu, D. G. Ma, *Chem. Commun.* **2011**, *47*, 3502.
- [25] C. J. Reckmeier, J. Schneider, A. S. Susha, A. L. Rogach, *Opt. Express* **2016**, *24*, A312.
- [26] K. Junka, J. Q. Guo, I. Filpponen, J. Laine, O. J. Rojas, *Biomacromolecules* **2014**, *15*, 876.
- [27] J. C. Bian, C. Huang, L. Y. Wang, T. Hung, W. A. Daoud, R. Q. Zhang, *ACS Appl. Mater. Interfaces* **2014**, *6*, 4883.
- [28] Z. Xie, F. Wang, C. Y. Liu, *Adv. Mater.* **2012**, *24*, 1716.
- [29] H. Q. Tao, K. Yang, Z. Ma, J. M. Wan, Y. J. Zhang, Z. H. Kang, Z. Liu, *Small* **2011**, *8*, 281.
- [30] R. L. Liu, D. Q. Wu, S. H. Liu, K. Koynov, W. Knoll, Q. Li, *Angew. Chem., Int. Ed.* **2009**, *48*, 4598.
- [31] X. T. Zheng, A. Ananthanarayanan, K. Q. Luo, P. Chen, *Small* **2015**, *11*, 1620.
- [32] Y. F. Wang, A. G. Hu, *J. Mater. Chem. C* **2014**, *2*, 6921.
- [33] A. W. Zhu, Q. Qu, X. L. Shao, B. Kong, Y. Tian, *Angew. Chem., Int. Ed.* **2012**, *51*, 7185.
- [34] J. C. Ge, Q. Y. Jia, W. M. Liu, L. Guo, Q. Y. Liu, M. H. Lan, H. Y. Zhang, X. M. Meng, P. F. Wang, *Adv. Mater.* **2015**, *27*, 4169.
- [35] Y. X. Fang, S. J. Guo, D. Li, C. Z. Zhu, W. Ren, S. J. Dong, E. K. Wang, *ACS Nano* **2011**, *6*, 400.
- [36] X. M. Li, Y. L. Liu, X. F. Song, H. Wang, H. S. Gu, H. B. Zeng, *Angew. Chem., Int. Ed.* **2015**, *54*, 1759.
- [37] X. Guo, C. F. Wang, Z. Y. Yu, L. Chen, S. Chen, *Chem. Commun.* **2012**, *48*, 2692.
- [38] Y. Wang, S. Kalytchuk, L. Y. Wang, O. Zhovtiuk, K. Cepe, R. Zboril, A. L. Rogach, *Chem. Commun.* **2015**, *51*, 2950.
- [39] M. Y. Sun, S. N. Qu, Z. D. Hao, W. Y. Ji, P. T. Jing, H. Zhang, L. G. Zhang, J. L. Zhao, D. Z. Shen, *Nanoscale* **2014**, *6*, 13076.
- [40] T. H. Kim, F. Wang, P. McCormick, L. Z. Wang, C. Brown, Q. Li, *J. Lumin.* **2014**, *154*, 1.
- [41] Y. H. Chen, M. T. Zheng, Y. Xiao, H. W. Dong, H. R. Zhang, J. L. Zhuang, H. Hu, B. F. Lei, Y. L. Liu, *Adv. Mater.* **2016**, *28*, 312.
- [42] W. Kwon, S. Do, J. Lee, S. Hwang, J. K. Kim, S. W. Rhee, *Chem. Mater.* **2013**, *25*, 1893.
- [43] C. Sun, Y. Zhang, K. Sun, C. Reckmeier, T. Q. Zhang, X. Y. Zhang, J. Zhao, C. F. Wu, W. W. Yu, A. L. Rogach, *Nanoscale* **2015**, *7*, 12045.
- [44] S. H. Song, M. H. Jang, J. Chung, S. H. Jin, B. H. Kim, S. H. Hur, S. Yoo, Y. H. Cho, S. Jeon, *Adv. Opt. Mater.* **2014**, *2*, 1016.
- [45] X. M. Li, M. C. Rui, J. Z. Song, Z. H. Shen, H. B. Zeng, *Adv. Funct. Mater.* **2015**, *25*, 4929.
- [46] M. J. Krysmann, A. Kelarakis, P. Dallas, E. P. Giannelis, *J. Am. Chem. Soc.* **2012**, *134*, 747.
- [47] P. C. Chen, Y. N. Chen, P. C. Hsu, C. C. Shih, H. T. Chang, *Chem. Commun.* **2013**, *49*, 1639.
- [48] P. Yu, X. M. Wen, Y. R. Toh, J. Tang, *J. Phys. Chem. C* **2012**, *116*, 25552.
- [49] S. N. Qu, D. Z. Shen, X. Y. Liu, P. T. Jing, L. G. Zhang, W. Y. Ji, H. F. Zhao, X. W. Fan, H. Zhang, *Part. Part. Syst. Character.* **2014**, *31*, 1175.
- [50] D. Zhou, H. Y. Zou, M. Liu, K. Zhang, Y. Sheng, J. L. Cui, H. Zhang, B. Yang, *ACS Appl. Mater. Interfaces* **2015**, *7*, 15830.
- [51] C. Sun, Y. Zhang, S. Kalytchuk, Y. Wang, X. Y. Zhang, W. Z. Gao, J. Zhao, K. Cepe, R. Zboril, W. W. Yu, A. L. Rogach, *J. Mater. Chem. C* **2015**, *3*, 6613.
- [52] Y. Wang, S. Kalytchuk, Y. Zhang, H. C. Shi, S. V. Kershaw, A. L. Rogach, *J. Phys. Chem. Lett.* **2014**, *5*, 1412.

Received: June 21, 2016  
Revised: November 1, 2016  
Published online: December 5, 2016